STRAIN RELATED PHENOMENA IN GaN THIN FILMS

C. Kisielowski, J.Krüger, S.Ruvimov, T.Suski, J. W. Ager III, E. Jones, Z. Liliental-Weber,

M.Rubin and E.R. Weber

Lawrence Berkeley National Laboratory and University of California, Berkeley, CA 94720

M. D. Bremser and R.F. Davis

Department of Materials Science and Engineering

North Carolina State University, Raleigh, NC 27695

ABSTRACT

Photoluminescence, Raman spectroscopy and x-ray diffraction are employed to demonstrate the coexistence of a biaxial and a hydrostatic strain that can be present in GaN thin films. The biaxial strain originates from growth on lattice mismatched substrates and from post-growth cooling. An additional hydrostatic strain is shown to be introduced by the presence of point defects. A consistent description of the experimental results is derived within the limits of the linear and isotropic elastic theory using a Poisson ratio $v = 0.23\pm0.06$ and a bulk modulus $B = 230\pm20$ GPa. These isotropic elastic constants help to judge the validity of published anisotropic elastic constants that vary greatly. Calibration constants for strain induced shifts of the near band edge PL lines with respect to the E_2 Raman mode are given for strain free, biaxially strained and hydrostatically contracted or expanded thin films. They allow to extract differences between hydrostatic and biaxial stress components if present. In particular, we determine that a biaxial stress of one GPa would shift the near band edge PL lines by 21 ± 2 meV and the E_2 Raman mode by 3.2 ± 0.3 cm^{-1} by use of the listed isotropic elastic constants. It is expected from the analyses that stoichiometric variations in the GaN thin films together with the design of specific buffer layers can be utilized to strain engineer the material to an extend that greatly exceeds the possibilities known from other semiconductor systems because of the largely different covalent radii of the Ga and the N atom.

I. Introduction

In recent years Gallium Nitride has attracted considerable attention because of the materials potential to fabricate bright UV- and visible light emitting diodes, power devices and LASER's [1,2,3]. Efforts in thin film growth led to a substantial improvement of heteroepitaxially grown GaN films [4]. Homoepitaxy became very recently possible by use of bulk-grown GaN as a substrate material [5,6]. The materials ability to tolerate unusual large extended defect densities (10^8 cm^{-2} and larger) without deterioration of physical properties such as the electroluminescence performance allows for an unprecedented technical progress. Details of the underlying physical processes, however, are not yet well understood.

Experimentally, GaN thin films and bulk crystals are often grown under extreme conditions: e.g. bulk GaN is grown around 1500°C under a hydrostatic nitrogen pressure of 1-2 GPa; MBE growth is performed at relative low temperatures (~700°C) to benefit from deviations from a thermodynamic equilibrium; the most commonly used substrates for heteroepitaxy are sapphire and SiC that may introduce large strain into the GaN layers because of a lattice mismatch of -13% and +4%, respectively [4]. Thus, strain and deviations from a stoichiometric composition of GaN certainly must be considered in order to understand the materials properties. Theoretical calculation performed up to now [7,8] do not yet account for this fact. They stress, however, that the native defect formation in GaN is strongly ruled by strain because of the significantly different covalent radii of the Ga and the N atoms [7]. Experimentally, large variations of the lattice parameters were observed and attributed to the incorporation of impurities and of non-stoichiometric native defects into the GaN lattice [9]. Very recently, a Ga supersaturation concentration was reported in bulk grown GaN crystals that may lead to the formation of Ga related defects or defect clusters such as precipitates of varying size or even Ga_N antisite defects in large concentrations (>1% locally) [10]. Moreover, it was realized that the thermal, biaxial strain introduced by different thermal expansion coefficients of the substrates and the GaN films introduces stresses that can lead to cracking of the brittle material [11] which hardly allows for plastic deformation. However, the presence of the thermal biaxial strain and the

hydrostatic strain induced by point defects are treated up to now as if they are separate issues that do not influence each other.

It is the purpose of this paper to point out the *coexistence* of the hydrostatic and the biaxial strain in GaN thin films. The external biaxial strain originates from the growth on lattice mismatched substrates and from the different thermal expansion coefficients of the GaN films and the substrates. Point defects introduce an internal hydrostatic strain that can be compressive or expansive depending on the size of the involved atoms. The strain is altered by the presence of buffer layers and of extended defects. Photoluminescence (PL), Raman and x-ray measurements are exploited to monitor strain. Results from GaN homoepitaxiy are used to obtain a zero strain calibration and the lattice parameters of the most perfect GaN films.

The paper is structured in the following manner. In section II we derive the required stress-strain relations for a coexisting biaxial and hydrostatic strain field by use of basic linear and isotropic elastic theory. The results of the modeling give guidance for the interpretation of the Raman, PL and x-ray diffraction measurements. In addition they help judging the validity of published anisotropic elastic constants that suffer from a large scatter. Experimental details are listed in section III. PL and Raman measurements are presented that document the presence of the coexisting strain fields. It is shown that the resulting hydrostatic and the biaxial stresses can uniquely be extracted from the relative shifts of the considered near band edge luminescence with respect to the E_2 Raman mode if an absolute stress calibration is provided (section III.1). This absolute calibration is obtained by comparing the PL and the Raman line positions with c-lattice constant measurements in section III.2. A dependence of the PL intensity of lines around 2.3 and 3.47 eV on the growth conditions and the defect density gives further evidence for a varying incorporation of (native) point defects into the GaN films that we expect to contribute to the strain variations (section III.3). Finally, the results will be discussed (section IV).

II. Stress-Strain Relations for Coexisting Hydrostatic and Biaxial Strain Fields

Principally, all necessary stress-strain relations for uniaxial, biaxial and hydrostatic

compression or tension can be obtained if the elastic constants of GaN were known within reasonable limits. However, this is not the case for GaN. Table I lists the published anisotropic elastic constants that vary greatly. For example, Detchprohm et al. [16] showed that for biaxial strain the ratio $\varepsilon_c/\varepsilon_a$ is given by $2s_{11}/(s_{11}+s_{12})$ were ε_c and ε_a are the strains along the GaN a- and c-axis and the s_{ij} are the elastic compliance's. In terms of elastic constants the ratio reads $\varepsilon_c/\varepsilon_a = -2\,c_{13}/c_{33}$. Numerically, the different elastic constants from table I give values $\varepsilon_c/\varepsilon_a = -1.18$ [12], -0.27 [13], -0.33 [14] and -0.53 [15] that vary by a factor of four.

In contrast, the isotropic elastic constants can be determined within moderate uncertainties. We review literature data to find values for the Bulk modulus B and the Poisson ratio v. A Bulk modulus $B = 230\pm20$ GPa can readily be extracted from recent publications [17,18]. The Poisson ratio is related to the quotient $\varepsilon_c/\varepsilon_a = [(c - c_0) / c_0] / [(a - a_0) / a_0]$. Here, a and c are the strained lattice constants of GaN and a_0, c_0 are reference values for stoichiometric and defect free GaN crystals. As to our knowledge, recent lattice parameter measurements of homoepitaxially grown GaN films [18] provide the most reliable values a_0 and c_0. They are listed in table I. These numbers are used to calculate $\varepsilon_c/\varepsilon_a$ from lattice parameter measurements published in references [9], [16] and [17]. Figure 1 summarizes the results. We find values $1.5 > \varepsilon_c/\varepsilon_a > -1.5$. Also, very few data exhibit values $0 < \varepsilon_c/\varepsilon_a < -0.5$ that one would expect if $\varepsilon_c/\varepsilon_a$ would equal the Poisson ratio. In fact, values $\varepsilon_c/\varepsilon_a$ from biaxially strained films are sometimes confused with the Poisson ratio [19]. If the films were biaxially strained, only, one would expect a constant value $\varepsilon_c/\varepsilon_a$. If we make the crucial assumption that in samples with a dominant biaxial strain [16,17] the different hydrostatic strain components average to zero, a mean value $\varepsilon_c/\varepsilon_a = -0.6 \pm 0.2$ is calculated from figure 1. This number will be used to determine the Poisson ratio. Thus, the reviewed strain ratios exceed both, the limit given by a hydrostatic compression ($\varepsilon_c/\varepsilon_a = 1$), and the limit given by a dominant biaxial strain. On the other hand, the data from reference [9] in figure 1 show that the growth rate or the doping with 10^{20} cm^{-3} of Zn initiate the changes in $\varepsilon_c/\varepsilon_a$. Thus, it seems that non-stoichiometric growth or the incorporation of atoms that differ in size from the Ga and the N atom cause the deviation of $\varepsilon_c/\varepsilon_a$ from a constant mean

value that we expect if the samples were biaxially strained, only.

Therefore, we choose to describe the coexistence of a biaxial and a hydrostatic strain field in terms of isotropic elastic theory. In this approximation the relation between stress and strain is [20]:

$$\varepsilon_i = E^{-1} \left(\sigma_i - \nu \left(\sigma_j + \sigma_k \right) \right) \tag{1}$$

where i,j,k label the stresses and the strains in the basal plane a,b and along the c axis. Shear components are neglected. In case of hydrostatic pressure ($\sigma_a = \sigma_b = \sigma_c = \sigma_p$) equation (1) reduces to:

$$\varepsilon_p = E^{-1} \sigma_p \left(1 - 2\nu \right) \tag{2}$$

and the ratio $\varepsilon_i / \varepsilon_j$ is one. For case of a biaxial stress in the basal plane ($\sigma_a = \sigma_b$, $\sigma_c = 0$) the relations are:

$$\varepsilon_a = E^{-1} \sigma_a \left(1 - \nu \right) \tag{3a}$$

$$\varepsilon_c = - E^{-1} \sigma_a \, 2\nu \tag{3b}$$

$$\varepsilon_c / \varepsilon_a = - 2\nu / \left(1 - \nu \right) \tag{3c}$$

It is clear from equation 3c that for a biaxial stress the measured lattice constants c and a are related to the Poisson ratio by $[(c - c_0) / c_0] / [(a - a_0) / a_0] = - 2\nu / (1-\nu)$. We use the value $\varepsilon_c / \varepsilon_a = 0.6 \pm 0.2$ from figure 1 to determine $\nu = 0.23 \pm 0.06$.

Strain induced by substitutional point defects can be introduced into the model considering Vegard's law that can be expressed by the equation:

$$\varepsilon = b \, C \tag{4a}$$

with $\Delta c / c_0 = \Delta a / a_0 = \varepsilon$, C = concentration of point defects and an expansion (contraction) coefficient b that was derived to be [21]:

$$b = 1/3 \left[1 - (r_s / r_h)^3 \right] N^{-1} \tag{4b}$$

Here, N is the concentration of lattice sites of the host matrix ($8.8 \; 10^{22} \; cm^{-3}$ Ga + N sites in GaN), r_h is the covalent tetrahedral radius of host atoms and r_s is the radius of solute atoms. Numerical values were given by Pauling [22] and they neglect lattice relaxation effects and the

ionicity of the constituents. The strain described by equations 3 and 4 can be linearly superimposed to give the effective strain values $\varepsilon_{c,eff} = [c - (c_o - \Delta c)] / (c_o - \Delta c)$ and $\varepsilon_{a,eff} = [a - (a_o - \Delta a)] / (a_o + \Delta a)$ that can be rewritten in the form:

$$\varepsilon_c = (1 - b\,C)\,(1 - 2\,\nu\,\sigma_a / E) - 1 \qquad\qquad (5a)$$

$$\varepsilon_a = (1 - b\,C)\,(1 + (1-\nu)\,\sigma_a / E) - 1 \qquad\qquad (5b)$$

Equations 5 allow to calculate the strain in the GaN films for varying biaxial stress if point defects of a given concentration are present. In figure 2a examples are given for the common substitution Si_{Ga} ($r_{Si} = 0.117$ nm, $r_{Ga} = 0.126$ nm) and for the two extreme substitutions Ga_N ($r_N = 0.07$ nm) and N_{Ga}. The elastic constants determine the slope of the lines and the incorporation of point defects induces a parallel line displacement. In addition, the largely different covalent radii of the Ga and the N atoms can easily cause changes of ε_c in the 10^{-3} range if the material is non-stoichiometric. Figure 2b depicts that $\varepsilon_c/\varepsilon_a$ reaches values $-1.5 < \varepsilon_c/\varepsilon_a < 1.5$ that exceed the limits of pure hydrostatic or pure biaxial strain and compare well with figure 1. Thus, $\varepsilon_c/\varepsilon_a$ greatly depends on the amount of biaxial stress, the concentration of impurities and the ratio r_s/r_h.

This work experimentally accesses such strain related phenomena by measuring the resulting stresses by PL and by Raman spectroscopy and the strains by x-ray diffraction.

III. Experimental

The 5 K photoluminescence (PL) was excited at 325 nm by a HeCd laser, analyzed by a double monochromator and detected by a lock-in amplifier. The 50 mW laser excitation power was kept constant to provide comparable results. In this paper, the crystalline quality of the GaN films is characterized by the full width at half maximum (FWHM) of the two crystal x-ray rocking curves. It is not attempted to extract defect concentrations from this values. Instead, we use an increasing FWHM as an indication for the degradation of the crystalline quality. c-lattice constants were measured with a Siemens D-5000 diffractometer equipped with a four bounce Ge

monochromator and a four circle translation capability. Unpolarized, local Raman measurements were performed at room temperature by focusing a 488 nm LASER beam to a 1 μm spot on the sample and detecting the back scattered light.

Samples grown by three different methods are considered in this study :

1) GaN films of ~0.5 μm thickness were grown by MBE at 675°C. Heteroepitaxy was performed on SiC and on sapphire c(0001)-planes, homoepitaxy on bulk GaN [23, 24]. The films were undoped and n-type. Low temperature (LT)-GaN buffer layers were typically grown around 500°C.

2) The two investigated n-type MOVPE films were deposited at 1030°C on AlN buffer layers. They were 3 - 5 μm thick and grown on sapphire a(11-20)-plane substrates. One of the samples was undoped and the other one doped with Si (3 10^{18} cm^{-3})[25].

3) n-type, ~3 μm thick MOCVD films were also deposited above 1000°C. In one case a LT-GaN buffer layer was deposited on sapphire [26] and in other experiments SiC c-plane substrates were used.

In none of the investigated thin films we observed cracks.

III.1 Photoluminescence and Raman studies

Figures 3a and 3b show the near band edge PL spectra of GaN grown on SiC and on sapphire. A collective displacement of the PL lines up to 30 meV can be seen. It is larger if GaN is grown on sapphire. Since the lines tend to broaden with increasing FWHM of the films, they overlap at some point in case of growth on SiC. In such a situation we determined the line position by fitting two Lorentzian lines to the data. In figure 3c we compare the PL spectrum of bulk-grown GaN with the one of a homoepitaxial film [24]: The differences are remarkable. While the MBE grown film exhibits a sharp donor bound exiton and negligible yellow luminescence, the 2.3 eV luminescence dominates greatly in bulk GaN and the band edge

luminescence is blue shifted and weak. TEM reveals a low dislocation density ($<10^7 cm^{-2}$) in the homoepitaxial film and no detectable dislocations in the bulk material near the substrate/film interface [27].

The energetic position of the near band edge exitons is plotted versus the FWHM of the x-ray rocking curves of GaN films grown on SiC with a LT-GaN buffer layer in figure 4a. The linear regression to the data emphasizes that the line displacements are not statistical but a collective shift that is attributed to the presence of stress. It is noted that the yellow luminescence band shifts even stronger but those data will be evaluated elsewhere. For comparison, the position of the donor bound exiton in a homoepitaxially grown sample is plotted, too, because it provides a calibration for strain free growth: PL energies of the donor bound exitons smaller than 3.467 eV indicate the presence of tensile stress, larger values indicate that the films are compressed.

In figure 4b we evaluate the PL data obtained from films grown on sapphire substrates with different buffer layers. It can be seen, that the growth of a LT-GaN buffer layer leads to an effective strain relaxation that is almost independent on the defect density and the growth method. In contrast, MBE growth of GaN films without buffer layers introduces large tensile stresses into films of poor crystalline quality. MOVPE growth on an AlN buffer layer introduces large compressive stresses. In these particular films, part of that large compressive stress could be caused by the larger lattice mismatch of the sapphire a-planes (20%) compared with the growth on c-planes that was used for the orientation of the substrates in all other cases. However, the near band edge PL lines of thin GaN films ($< 10\mu m$) grown on sapphire c-planes with AlN buffer layers also appear at energies as large as 3.48 to 3.49 eV as documented in an earlier study [28]. Thus, the growth on an AlN buffer layer may introduce larger stresses than the growth on a LT-GaN buffer layer in spite of the similar growth temperature ($\sim 1030^\circ C$) of the MOVPE and the MOCVD films. Since in addition the MBE growth on an LT-GaN buffer layer proceeds at only $675^\circ C$ and yet results in a similarly low strained GaN film, we conclude that, beside the different thermal expansion coefficients of GaN and sapphire, details of the buffer layer growth

8

must modify the stress in the GaN films greatly.

There are several sources that can cause confusion as to a physical identification of PL transitions and the origin of their shift: different donor bound exitons have been observed in the near band edge region [29,30]; free exitonic transitions are commonly observed [5, 29, 30]; the near band edge PL line shifts can be caused by the Burstein-Moss effect rather than by strain [31]. Therefore, we support our assignment of the PL line shifts to the presence of stress by performing Raman measurements of the E_2 Raman mode that is known to be shifted by stress, only [32]. The three examples of figure 5 depict the presence of a tensile stress in a film grown on SiC and a larger compressive stress in a GaN film grown on sapphire. However, the E_2 line position varies almost continuously even if different samples were grown at the same temperature. Again, the stress cannot exclusively be determined by the thermal expansion coefficients of the films and the substrates. Moreover, the E_2 Raman mode of homoepitaxially grown GaN and the investigated bulk grown GaN appears at an identical wave number of 566.2 cm^{-1}. We take this number as a reference for unstressed films. However, it is noted that the lattice constant of bulk GaN may locally vary[18] which is why this identity can be accidental.

Next, a calibration of the Raman and the PL line shifts is established for stress free, biaxially and hydrostatically stressed samples. Again, we assume that the homoepitaxially MBE grown GaN film deposited on bulk GaN is not biaxially strained because of the identical thermal expansion coefficients of the film and the substrate. The donor bound exiton energy $E_o = 3.467$ eV and the E_2 Raman mode at $\omega_o = 566.2$ cm $^{-1}$ determine the calibration constant $k = E_o/\omega_o = 6.12 \ 10^{-3}$ eV cm. For biaxially stressed films, a relation $E(\sigma_a) = k_a \ \omega(\sigma_a)$ is expected where σ_a is a biaxial stress. Therefore, we plot in figure 6 the energy position of the donor bound exitons versus the measured position of the E_2 Raman mode for our samples that exhibit different amounts of shifts. A linear regression to the data yields the calibration constant $k_a = 6.6 \ 10^{-3}$ eV cm. The scatter of the data in figure 5 was checked to be caused by a lateral inhomogeneities in the GaN films. Finally, a hydrostatic pressure σ_p has been measured to shift the E_2 Raman mode by $\omega = \omega_o + 3.6$ cm^{-1} GPa^{-1} σ_p and the near band edge PL lines by $E = E_o + 40$ meV GPa^{-1} σ_p [33,34]. The ratio $k_p = 40$ meV GPa $^{-1}$ / 3.6 cm^{-1} GPa^{-1} = 1.1 10^{-2} eV cm i s the calibration

constant for the hydrostatic case. The relation $E(\sigma_p) = k_p\, \omega(\sigma_p)$ is depicted in figure 6, too. k_p is almost twice as large as k_a measured in our experiments. We assign this discrepancy to the biaxial nature of the stresses σ_a in the GaN films. It can be seen from the figure that most of the experimental data are influenced by both a hydrostatic and a biaxial strain component as one would expect from the review of the data presented in figure 1.

Principally, the results presented in figure 6 allow for an extraction of differences between hydrostastic and biaxial stresses by projecting the data points on each of the straight lines. Figure 6 gives an example. It refers to the Si doped and undoped MOVPE grown samples. It can be seen that both samples hold a similar amount of biaxial stress $\sigma_a = 0.6$ GPa. In contrast, the Si doped sample exhibits a reduction of σ_p by less than 0.1 GPa.

Obviously, the procedure requires an absolute calibration of the hydrostatic and biaxial stresses. This calibration is readily given for the hydrostatic pressure because σ_p has been measured to shift the PL lines by 40 meV GPa^{-1} and the E_2 Raman mode by 3.6 cm^{-1} GPa^{-1}. The biaxial stress is calibrated in the next section but the result is already indicated in figure 6.

III.2 Absolute Calibration of the Biaxial Stress

The PL and the Raman line shifts are compared with c-lattice constant measurements in figures 7a and 7b. A large scatter of the data can be seen. We expect that equation 3b is valid. A linear relation between the biaxial stress σ_a and the Raman and PL line shifts is assumed: $\sigma_a = -\Delta\omega\,/\,k_{Ra,a}$ and $\sigma_a = -\Delta E\,/\,k_{PL,a}$. Here the negative sign accounts for a positive line shift that is induced by a negative (compressive) stress. $k_{Ra,a}$ and $k_{PL,a}$ are the absolute calibration constants for the Raman shift $\Delta\omega$ and the PL line shift ΔE induced a biaxial stress. Thus, we expect the relations $\varepsilon_c = E^{-1}\,2\,\nu\,\Delta\omega\,/\,k_{Ra,a}$ and $\varepsilon_c = E^{-1}\,2\,\nu\,\Delta E\,/\,k_{PL,a}$ to be valid for films with a dominant contribution of a biaxial stress to the line shifts. A linear regression to those data in figures 7 that do not significantly deviate from a straight line yields: $\varepsilon_c = (3.8 \pm 0.4)\,10^{-4}$ cm $\Delta\omega$ and $\varepsilon_c = (0.059 \pm 0.006)$ eV ΔE for the Raman and the PL measurements, respectively. It can be seen

from figures 7 that both linear regressions closely match the zero calibration point given by the homoepitaxially grown GaN films. A comparison with figure 2a reveals that in this case all of the evaluated films are mainly biaxially strained. On the other hand, the data which were excluded from the regression can be described by parallel straight lines and their offset is attributed to an incorporation of point defects with tetrahedral covalent radii that are either smaller or larger than the radii of the host atoms (compare with equation 5a and with figure 2b).

The slopes of the lines and the isotropic elastic constants from table I determine $k_{Ra,a}^{-1} =$ (3.2 $\pm$ 0.3) cm $^{-1}$ GPa^{-1} and $k_{PL,a}^{-1} =$ (21 $\pm$ 2) meV GPa^{-1} . The uncertainties in B and ν are neglected in the given error bars. The quotient $k_{PL,a}$ / $k_{Ra,a} =$ 6.6 10^{-3} eV cm equals $k_a=$ 6.6 10^{-3} eV cm that was determined from figure 5. Thus, we obtained consistency between the quotient of the absolute calibration constants $k_{PL,a}$ / $k_{Ra,a}$ obtained from x-ray measurements with the relative calibration constant k_a deduced from the direct comparison of the PL and Raman measurements. In particular, the values $k_{PL,a}^{-1}$ and $k_{Ra,a}^{-1}$ scale the biaxial strain in figure 6 absolutely.

III.3 PL Intensity Measurements

Further evidence for a varying concentration of point defects in the investigated samples comes from intensity measurements. The intensity ratio of the yellow luminescence band at 2.3 eV and the near band edge luminescence of the GaN films is analyzed. These luminescence lines are of special interest because of their possible relation to the presence of native point defects [10, 34]. The lines are observed in bulk -, MBE - , MOCVD- and MOVPE grown samples. This supports the intrinsic character of the defects that give rise to the PL lines. Figure 5 reveals that their ratio varies the most in case of high quality GaN films (FWHM<10 arc min): in homoepitaxially MBE grown GaN the yellow luminescence can drop down to the detection limit or appear at medium ratios depending on the growth conditions; in the MOVPE crystals, medium ratios were detected, too; in bulk GaN the ratio is the largest. Thus, the defect introduction depends on growth parameters. In crystals with poorer quality the ratio scatters also

considerably. On the average, however, it is smaller if the GaN films were grown on SiC. This was reported earlier for a growth series that compared GaN growth on SiC with growth on sapphire [35]. The average ratio drops with degrading crystalline quality. Therefore, the PL spectra of crystals with very poor quality may also exhibit only near band edge luminescence and no yellow luminescence band.

IV. Discussion and Conclusion

Our experiments were triggered by the observed large strain induced shifts of the near band edge PL that causes confusion as to an identification of the involved transitions. However, attempts to understand the phenomena soon revealed serious limitations such as the inconsistency of the anisotropic elastic constants (table I) or the unexpected variation of the $\varepsilon_c/\varepsilon_a$ values (figure 1) that does not even change if the films crack [16]. In particular it is the range of the measured $\varepsilon_c/\varepsilon_a$ ratios that made us doubt the common believe that it is only the biaxial strain which is responsible for the spectroscopic line shifts.

The presented model rationalizes the large scatter of $\varepsilon_c/\varepsilon_a$. We stress four facts. First, the anisotropic elastic constants can be compared with the experimentally deduced isotropic elastic constants by calculating the Poisson ratio, the Young - (E) and the bulk (B) modulii in the Voigt average from the anisotropic elastic constants [36] (z along the c-axis and x,y in the basal plane). They are listed in table one. It can be seen that the data from references [13] and [15] compare well with our values. Moreover, the ratio $\varepsilon_c/\varepsilon_a = - 2\ c_{13}/c_{33} = -0.54$ from reference [15] agrees closely with our isotropic estimation $\varepsilon_c/\varepsilon_a = - 2\ v\ /\ (1 - v) = - 0.6 + 0.2$ extracted from figure 1. Thus, we find the best agreement of our isotropic elastic constants with the anisotropic elastic constants from reference [15]. Second, the factor $[-2\ v\ /\ (1 - v)\ ]$ determines $[(c - c_0)\ /\ c_0]\ /\ [(a - a_0)\ /\ a_0]$ in the absence of point defects (figure 2b). It is the presence of non-stoichiometric defects or impurities that makes $\varepsilon_c/\varepsilon_a$ vary greatly. This limits the accuracy as to which v can be determined by measuring the lattice constants c and a of GaN thin films if the stoichiometry is uncertain. Third, it is the unusual large difference of the covalent tetrahedral radii of Ga and N

12

that can cause large changes of the lattice constants in case of a moderate introduction of non-stoichiometric defects or impurities. Finally, homoepitaxial growth of GaN recently provided benchmark values for crucial parameters such as the zero stress value for the donor bound exiton [5, 24] and the E_2 Raman mode or for the reference lattice constants a_o and c_o [16].

The presented data analysis assumes a statistical fluctuation of the hydrostatic strain components that are induced by point defects in those samples that exhibit a dominant biaxial stress. We calculate the mean value $\varepsilon_c/\varepsilon_a = -0.6 + 0.2$ and the slopes in figures 6 $\varepsilon_c = (3.8 \pm 0.4)$ 10^{-4} cm $\Delta\omega$ and $\varepsilon_c = (0.059 \pm 0.006)$ ΔE with this assumption. Its validity is supported by the result of the linear regressions in figure 6 which closely match the zero calibration point provided by homoepitaxial growth. This would be difficult if the point defects in the investigated samples would induce a hydrostatic strain that is not zero on the average.

At present, the proposed model allows for a qualitative comparison with experimental data, only, because of various reasons. First, any uncertainty in the isotropic elastic constants strongly modifies the given calibration constants. This is demonstrated for the Raman calibration constant $k_{Ra,a}$ in table II. The first line lists the values we consider best. In the second line we calculated $k_{Ra,a}$ with a Poisson ratio $\nu = 0.37$ which is used in literature (table I). It can be seen that this 60% change of ν causes $k_{Ra,a}$ to change by 240%! In the third line we use the elastic constants from reference [37]. $k_{Ra,a} = 6.2$ cm^{-1} was reported there. It can be seen that we would calculate a comparable large value of 8.1 cm^{-1} from these elastic constants. Therefore, we conclude that it is the poor knowledge of the elastic constants that induces the largest uncertainties. The experimental uncertainty in $\nu = 0.23 \pm 0.06$ provided in this paper still exceed the uncertainties obtained from the measurements of figure 6 that give $k_{Ra,a} = (3.2 \pm 0.3)$ cm^{-1} GPa^{-1} and $k_{PL,a}^{-1} = (21 \pm 2)$ meV GPa^{-1} if we neglect the uncertainties in ν and B. Second, the calculation of the lattice expansion/contraction induced by point defects neglects lattice relaxation effects and the ionicity of the constituents. Thus, it will systematically overestimate the size effect.

In figure 6 we show that a hydrostatic and a biaxial stress can uniquely be determined from the PL and the Raman measurements. Physically, we distinguish between them because the

biaxial stress is induced through the substrate but the additional hydrostatic strain variations by the presence of point defects. Principally, however, the biaxial stress can be decomposed into a hydrostatic stress and a uniaxial stress which is why the information about hydrostatic components of different origins is mixed in figure 6. Again modeling is required to extract useful information. This problem will be treated elsewhere because, at present, the poor quality of the GaN films causes broadening of the PL transitions and thereby line superposition's that give rise to hardly controllable uncertainties which we expect to decrease rapidly with improving crystal quality of the GaN films.

Our analyses does not explicitly address strain relaxation processes that are induced by buffer layers or by dislocation networks. The lattice mismatch, the thermal strain and the effect of buffer layers and of dislocation networks on the lattice relaxation are simply expected to modify measured biaxial stresses. However, it is of practical importance for crystal growth to realize that the growth of a LT-GaN buffer layer relaxed the stresses most efficently in our investigated samples (figure 3b) for reasons that are currently under investigation.

We focused our study on investigating the influence of point defects on the lattice parameters. Evidence for the modification of the biaxial strain comes from the largely varying values of ε_c and $\varepsilon_c/\varepsilon_a$ in figures 1 and 7. Further evidence is presented by measuring the intensity of the near band edge PL and the yellow luminescence (figure 8). The presence of these PL lines in extended defect free areas of bulk grown GaN [10, 27] links them with point defects or defect clusters that can be inhomogeneously distributed if extended defects are present [27, 38]. Since they appear in all investigated samples, they seem to be of intrinsic origin or related to a common impurity. Usually, it is the strain field around dislocations with edge character that interacts with point defects to form a Cotrell atmosphere [36]. Thus, the inhomogeneous distribution of the luminescence intensity can be the result of either the two processes that minimize the strain energy: either point defects are gettered around dislocations or they are preferentially formed during growth to locally or globally relax strain.

In conclusion we show for the first time that in GaN thin films the superposition of a hydrostatic and a biaxial strain field determines the observed stress. A hydrostatic strain is

14

induced by the presence of point defects and the biaxial strain by the growth on lattice mismatched substrates with different thermal expansion coefficients. The presence of both strain fields limits the accuracy as to which elastic constants can be determined. A consistent description of PL, Raman and x-ray diffraction measurement is presented that uses a best estimation of the bulk modulus B = 230$\pm$20 GPa and of the Poisson ratio ν = 0.23 $\pm$ 0.06. Only one set of published anisotropic elastic constants [15] agrees best with these isotropic elastic constants. Homoepitaxial growth of GaN provides calibration constants for stress free samples. A procedure to determine differences between the biaxial and the hydrostatic stress from the PL and Raman measurements is presented. In particular, we find that a biaxial stress of one GPa would shift the E_2 Raman mode by (3.2 $\pm$ 0.3) cm^{-1} GPa^{-1} and the near band edge PL lines by (21 $\pm$ 2) meV GPa^{-1}. The dependence of these values on the isotropic elastic constants is given. Experimental evidence is presented that indicates a varying concentration of (native) point defects in the GaN films grown by different methods. A dependence of the biaxial stress on the buffer layer growth conditions and its modification by an intentional incorporation of (native) point defects seem to allow for strain engineering of GaN films.

Acknowledgments

References:

[1] S. Nakamura, M. Senoh, N. Iwasa, S. Nagahama, Jpn. J. Appl. Phys. Lett. **34** , L797 (1995)

[2] M.A. Kahn, A. Bhattarai, J.N. Kuznia, D.T. Olsen, Appl. Phys. Lett. **63** , 1214 (1993)

[3] S. Nakamura, M. Senoh, S. Nagahama, N. Iwasa, T. Yamada, T. Matsushita, H. Kiyoku, Y. Sugimoto, Jpn. J. Appl. Phys. **35**, L217 (1996)

[4] H. Morkoc, S.Strite, G.B.Gao, M.E. Lin, B. Sverdlov, M. Burns, J. Appl. Phys. **76** , 1363 (1994)

[5] K. Pakula, A. Wysmolek, K.P. Korona, J.M. Baranowski, R. Stepniewski, I. Grzegory, M. Bockowski, J. Jun, S. Krukowski, M. Wroblewski, S. Porowski, Proceedings of the NATO Advanced Research Workshop, Head 95, Smolonica, Slovakia

[6] F.A. Ponce, D.P. Bour, W. Götz, N.M. Johnson, H.I. Helava, I. Grzegory, J. Jun, S. Porowski, Appl. Phys. Lett. **68** , 917(1996)

[7] J. Neugebauer and C.G. Van de Walle, Phys. Rev. **B50**, 8067 (1994)

[8] P. Boguslawski, E. Briggs, and J. Bernholz, Phys. Rev. **B51**, 17255 (1995)

[9] O. Lagerstedt, B. Monemar Phys. Rev. **B19**, 3064 (1979)

[10] Z. Liliental-Weber, C. Kisielowski, X. Liu, L. Schloss, J. Washburn, E.R. Weber, I. Grzegory, M. Bockowski, J. Jun, T. Suski, S. Porowski, Solid State Electronics, 1995, in press

[11] K. Hiramatsu, T. Detchprohm, I. Akasaki, Jpn J. Appl. Phys. **32**, 1528 (1993)

[12] V.A. Savastenco, A.U. Sheleg, Phys. Status Solidi (a) **48**, K135 (1978)

[13] K. Kim, W.R.L. Lambrecht, B. Segall, Phys. Rev. **B50**, 1502 (1994)

[14] T. Azuhata, T. Sota, K. Suzuki, J. Phys.: Condens. Matter **8**, 3111 (1996)

[15] A. Polian, M. Grimsdich, I. Grzegory, J. Appl. Phys. **79**, 3343 (1996)

[16] T. Detchprohm, K. Hiramatsu, K. Itoh, I. Akasaki, Jpn, J. Appl. Phys. **31**, L1454 (1992)

[17] M. Leszczynski, T. Suski, P. Perlin, H. Teisseyre, I. Grzegory, M. Bockowski, J. Jun, S. Porowski, J. Major, J. Phys. D: Appl. Phys. **20**, A149 (1995)

[18] M. Leszczynski, H. Teisseyre, T. Suski, I. Grzegory, M. Bockowski, J. Jun, S. Porowski, K. Pakula, J.M. Baranowski, private communication

[19] W. Riger, T. Metzger, H. Angerer, R. Dimitrov, O. Ambacher, M. Stutzmann, Appl. Phys. Lett. **68**, 970 (1996)

[20] e.g. A. Kelly, G.W. Groves, " Crystallography and Crystal Defects" Adison-Wesley Pub. Comp. 1970

[21] Y.T. Lee, N. Miyamoto, J.-I. Nishizawa, J. Electrochem. Soc. **122**, 530 (1975)

[22] L. Pauling "The Chemical Bond", Cornell University Press 1967

[23] N. Newman, J. Ross, M. Rubin, Appl. Phys. Lett. **62**, 1242 (1993)

[24] A. Gassmann, T. Suski, Z. Liliental-Weber, N. Newman, C. Kisielowski, E. Jones, E.R. Weber, M.D. Rubin, H.I. Helava, I. Grzegory, M. Bockowski, J. Jun, S. Porowski, J. Appl. Phys. **80**, 1996, in press

[25] S. Ruvimov,.Z. Liliental-Weber, T. Suski, J.W. Ager III, J. Washburn, J. Krüger, C. Kisielowski, E.R. Weber, H. Amano, I. Akasaki, Appl. Phys. Lett. 1996, in press

[26] S. Nakamura, M. Senoh, N. Iwasa, S. Nagahama, T. Yamada, T. Mukai, Jpn. J. Appl. Phys. **34**, L1332 (1995)

[27] Z. Liliental-Weber, S. Ruvimov, C. Kisielowski, Y. Chen, W. Swider, J. Washburn, N. Newman, A. Gassmann, X. Liu, L. Schloss, E.R. Weber, I. Grzegory, M. Bockowski, J. Jun, T. Suski, K. Pakula, J. Baranowski, S. Porowski, H. Amano, I. Akasaki, MRS Symposia Proceedings **395**, 1996, in press

[28] H. Amano, K. Hiramatsu, I. Akasaki, Jpn. J. Appl Phys. **27**, L1384 (1988)

[29] D. Volm, K. Oettinger, T. Streibel, D. Kovalev, M. Ben-Chorin, J. Diener, B. K. Meyer, J. Majewski, L. Eckey, A. Hoffmann, H. Amano, I. Akasaki, K. Hiramatsu, T. Detchprohm, sub. Phys. Rev. B. (1996)

[30] C. Merz, M. Kunzer, U. Kaufmann, I. Akasaki, H. Amano, Semiconductor Science and Technology 11, 712 (1996)

[31] H. Teisseyere, P. Perlin, M. Leszcynski, T. Suski, I. Grzegory, J. Jun, S. Porowski, T.D. Mustakas, J. Appl. Phys. **76**, 2429 (1994)

[32] P.Perlin, C. Jauberthie-Carillon, J.P. Itie, A.S. Miguel, I. Grzegory, A. Polian, Phys. Rev. **B45**, 83 (1992)

[33] P. Perlin, T. Suski, H. Teisseyre, M. Leszczynski, I. Grzegory, J. Jun, S. Porowski, P. Boguslawski, J. Bernholc, J.C. Chervin, A. Polian, and T.D. Moustakas, Phys. Rev. Lett. **75**, 296 (1995)

[34] P. Perlin, I. Gorczyca, N.E. Christiansen, I. Grzegory, H. Teisseyre, T. Suski, Phys. Rev. **B45**, 13307 (1992)

[35] T.C. Fu, N. Newman, E. Jones, J.S. Chan, X. Liu, M.D. Rubin, N.W. Cheung, E.R. Weber, J. Elec. Mat. **24**, 249 (1995)

[36] e.g. J.P. Hirth and J. Lothe "Theory of Dislocations", McGraw-Hill, New York 1960

[37] T. Kozawa, T. Kachi, H. Kano, H. Nagase, M. Koide, K. Manabe, J. Appl. Phys. **77**, 4389 (1995)

[38] F.A. Ponce, D.P. Bour, W. Gotz, P.J. Wright, Appl. Phys. Lett. **68**, 57 (1996)

Tables:

Table 1:

Anisotropic and isotropic elastic constants considered in this paper. References are indicated. B = Bulk modulus, E = Young modulus, ν = Poisson ratio. The listed isotropic elastic constants were calculated in the Voigt average [36] from the c_{ij}. Our best estimation of the experimentally determined isotropic elastic constants and of lattice parameters of GaN are listed, too.

Table 2:

A dependence of the Raman calibration factor $k_{Ra,a}$ on the isotropic elastic constants is given by equation 3b. In the Table, we evaluate the effect of different isotropic elastic constants on the Raman calibration factor. Typical values from literature are taken. For details see text.

Figure captions:

Figure 1:

Evaluation of literature data $\varepsilon_c/\varepsilon_a$. References are given. A mean value $\varepsilon_c/\varepsilon_a$ is calculated from samples that exhibit a large biaxial stress. It can be seen that the literature data exceed both limits given by a pure hydrostatic strain and a dominant biaxial strain. The values are influenced by doping and by the rate at which the GaN films are grown.

Figure 2a:

Calculated dependence of ε_c on the biaxial stress σ_a for selected point defects of the given concentration. Equation 5a was used. It can be seen that the coexisting hydrostatic and biaxial strain fields induce a parallel displacement of the lines that is positive if the size of the impurities exceeds the size of the host atom. The slope of the lines is determined solely by the elastic constants.

Figure 2b:

Calculated dependence of $\varepsilon_c/\varepsilon_a$ on the biaxial stress σ_a for the selected point defects of the given concentration. Equations 5 were used. It can be seen that the coexisting hydrostatic and biaxial strain fields easily induce changes $-1.5 < \varepsilon_c/\varepsilon_a < 1.5$. A comparison with figure 1 directly reveals that the observed experimental scatter is explained by this effect. Numbers depend on the size of the atoms and their concentration. In case of a stoichiometric and undoped crystal one would expect a constant value that was chosen to be 0.6 because of the results presented in figure 1. This value is related to the Poisson ratio by equation 3c.

Figure 3a:

5K PL spectra of GaN films on SiC. LT-GaN buffer layers were grown. A collective displacement of the PL lines by ~10 meV is seen. The x-ray FWHM characterizes the crystalline quality of the films. There is a tendency that films grown on SiC exhibit a red shift of the PL lines.

Figure 3b:

5K PL spectra of MBE grown GaN films on sapphire. No buffer layers were grown. A collective displacement of the PL lines by ~30 meV is seen. There is a tendency that films grown on sapphire exhibit a blue shift of the PL lines.

Figure 3c:

5K PL spectra of a homoepitaxially MBE grown GaN film on bulk GaN. The thin film exhibits almost only donor bound exitonic transitions and very weak yellow luminescence that, in contrast, dominates the PL spectrum of the bulk crystal. A large blue shift of the weak near band edge luminescence is observed in bulk GaN. Out of all investigated crystals, only the bulk crystals exhibit a large blue shift of the near band edge PL that is caused by the large n-doping ($~10^{20}$ cm^{-3}).

Figure 4a:

Energetic position of the two PL transitions from figure 1a observed in films with different crystalline quality that degrades with increasing FWHM of the x-ray rocking curves. All samples were grown on SiC c-planes. LT-GaN buffer layers were grown. The linear regression emphasizes the collective shift of the lines.

Symbols:

Open symbols: Donor bound exitons; filled symbols: Line of unknown origin.

Circles: MBE heteroepitaxy; square: MBE homoepitaxy; triangles: MOCVD heteroepitaxy

Figure 4b

Energetic position of the donor bound exitonic luminescence from figure 1b observed in films with different crystalline quality that degrades with increasing FWHM of the x-ray rocking curves. The films were grown on sapphire and typically on c-planes. It is seen that the position of the luminescence is determined by the choice of the buffer layers that greatly modifies the stress. Homoepitaxy provides a standard for stress free growth. A red shift is caused by tensile stress

21

and a blue shift by compression.

Symbols:

Open circles: MBE films grown on a LT-GaN buffer layer.

Filled circles: MBE films grown without a buffer layer.

Triangles: MOCVD grown films on a LT-GaN buffer layer from two different sources.

Filled square: Homoepitaxially MBE grown film.

Open squares: MOVPE films grown on sapphire a-planes and on an AlN buffer layer [16]. The undoped sample exhibits a larger blue shift than the doped one (Si: $3 \cdot 10^{18} cm^{-3}$)

Figure 5:

Position of the E_2 Raman mode in bulk GaN single crystals and in films grown on SiC and on sapphire. Homoepitaxially grown MBE films and bulk GaN exhibit a position of the E_2 Raman mode at 566.2 cm $^{-1}$ (stress free standard). The shifts of the line position is caused by a tensile stress in the film grown on SiC and compressive one if grown on sapphire.

Figure 6

Plot of the donor bound PL energy versus the position of the E_2 Raman mode. A linear regression to the data yields the calibration constant $k_a = 6.6 \cdot 10^{-3}$ eV cm (solid line). The dashed line is calculated from the known hydrostatic pressure dependence of the PL and the Raman lines ($k_p = 1.1 \cdot 10^{-2}$ eV cm). The homoepitaxial film (open square) provides the calibration for the stress free case. The absolute stress calibration is given for one GPa. In the absence of experimental errors, a difference between the biaxial and the hydrostatic stress can be determined by the indicated projections on the straight lines as indicated for the two MOVPE samples (squares).

Figure 7a:

Plot of (c - c_0) / c_0 versus the Raman shift of the E_2 mode. A positive Raman shift indicates compressive (negative) stress. The bold straight line is fitted to achieve an absolute calibration of

the biaxial stress. Data close to the thin lines were excluded from fitting. The parallel displacement of such data points is attributed to large hydrostatic strain fields caused by point defects. A positive line displacement is caused by the larger size of solute atoms compared with host atoms ($r_S > r_h$). Filled circles: this work. Filled squares: data extracted from reference [19]. Open square: homoepitaxial MBE growth.

Figure 7b:

Plot of $(c - c_0) / c_0$ versus the shift of the exitonic luminescence. The plot compares with figure 7a.

Figure 8:

Intensity ratio of the yellow luminescence band and the donor bound near band edge PL lines in films with different crystalline quality that degrades with increasing FWHM of the x-ray rocking curves.

Symbols:

Filled squares: MBE grown films on SiC and bulk GaN.

Filled circles: MBE grown films on sapphire.

Filled triangle: bulk GaN.

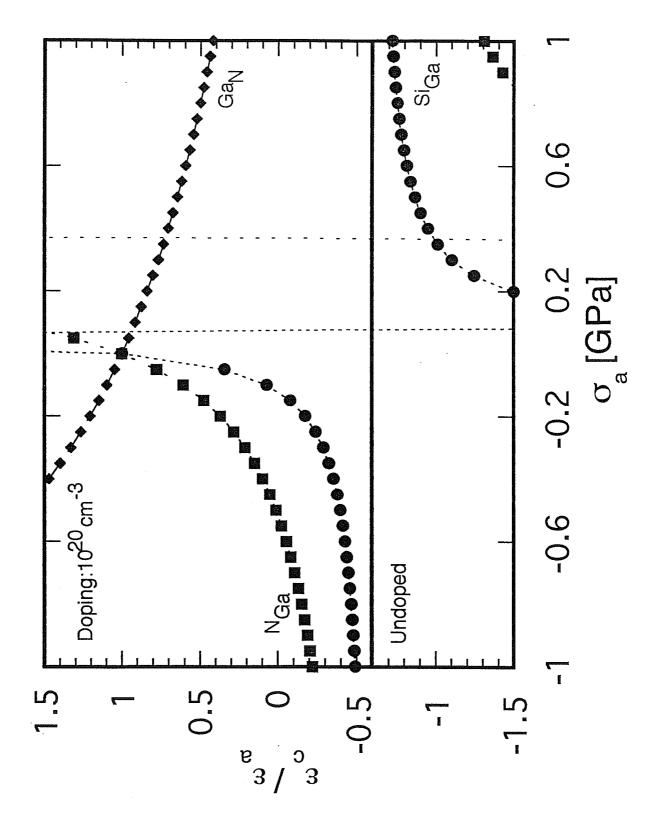Crossed squares: MOVPE films grown on sapphire a-planes.

Table I

Elastic Constants [GPa] and Lattice Parameters of GaN

Anisotropic:

Isotropic:

c_{11}	c_{12}	c_{13}	c_{33}	c_{44}	B	E	ν	
296	130	158	267	24	190	148	0.37	[12]
396	144	64	476	91	201	314	0.24	[13]
369	94.2	66.7	397	118	180	324	0.20	[14]
390	145	106	398	105	243	305	0.26	[15]

Experimental Values: 230±20 ~370 0.23±0.06 [15,16,17,18]

Lattice constants [nm] : a = 0.31878 c = 0.51850 [18]
± 0.00003 ± 0.00002

Table II

Poisson ratio	Bulk modulus [GPa]	Young modulus [GPa]	Raman factor [(GPa cm)$^{-1}$]
0.23	230	370	3.2
0.37	230	180	10.8
0.30	163	196	8.1

Hydrostatic strain:
$\varepsilon_c / \varepsilon_a = 1$

Biaxial strain:
$\varepsilon_c / \varepsilon_a = -2\nu / (1-\nu)$

Zn
Doping

Growth
Rate

[9]   [9]   [17]   [16]

References

$\varepsilon_c / \varepsilon_a$

1.5   1   0.5   0   -0.5   -1   -1.5

Fig 1
Kisielowski

Fig 2a

$\epsilon_c = (c - c_0) / c_0$

σ_a [GPa]

Doping: 10^{20} cm^{-3}

Ga$_N$

Undoped

Si$_{Ga}$

N$_{Ga}$

Doping:10²⁰ cm⁻³

Ga_N

N_Ga

Undoped

Si_Ga

$\varepsilon_c / \varepsilon_a$

σ_a [GPa]

Fig 2b
Kisielowski

Fig. 3a

XRC FWHM = 25 arcmin ⟶

XRC FWHM = 16 arcmin ⟶

PL-Intensity [a.u.]

Energy [eV]

3.20 3.25 3.30 3.35 3.40 3.45 3.50 3.55 3.60

Figure 36

Fig. 3c
Wisielowski

Fig 4a

Fig 4b

GaN E$_2$ phonon

Fig 5

fig 6.

Fig. 7a:

Fig 7b

Fig. 8
Ivan Januchit